GOME moon measurements, including instrument characterisation and moon albedo

Marcel R. Dobber Space Research Organisation Netherlands (SRON)
Sorbonnelaan 2, 3584 CA Utrecht, The Netherlands
phone: +31-30-2535722 fax: +31-30-2540860
e-mail: M.Dobber@sron.ruu.nl
url: http://www.sron.ruu.nl

Abstract

In this paper the moon spectra observed by GOME are examined in detail. For the moon observations this paper presents the first analysis of spectra and all factors that contribute to the measured signal are analysed in detail. It is shown that the moon spectra, in addition to the sun spectra, can be used for monitoring of the instrument performance. The geometrical moon albedo over the complete 240-800 nm wavelength range as measured by GOME is presented and discussed.

Keywords: GOME, moon, albedo, calibration, degradation.

1. Introduction

The Global Ozone Monitoring Experiment (GOME) was launched in April 1995, on the second European Remote Sensing Earth observation satellite (ERS-2). In order to maintain proper wavelength and radiometric calibration of the instrument the sun, moon, and an on-board spectral lamp are employed. This paper focuses on the moon observations performed with GOME. The sun is the most important and most stable in-orbit calibration source and GOME sun observation results have been presented previously [Refs 2,4]. The GOME moon observations serve two purposes: firstly to measure and characterise the instrument performance and degradation and secondly to study the moon itself with a satellite based instrument. Both aspects are also of interest to the successor of GOME, SCIAMACHY (SCanning Imaging Absorption spectroMeter for Atmospheric CartograpHY), to be launched as part of the ENVISAT environmental satellite in 1999. Details on the GOME instrument and its design can be found elsewhere [Ref 1]. The main operational mode of GOME observes the earth and its atmosphere in (near)nadir direction. For calibration purposes the sun can be observed directly. In this case the irradiance of the sun is directed via a reflective diffuser (wet sand blasted aluminium) towards the spectrometer. To protect the diffuser as much as possible a solar mesh (transmittance 0.196) is placed in front of the diffuser. The sun-over-diffuser spectra provide all necessary information to perform an absolute radiometric calibration of the nadir earth radiance spectra and check the wavelength calibration using solar Fraunhofer lines. The moon provides an independent irradiance source that can be used for calibration and characterisation purposes. The moon is viewed over the nadir scan mirror at an incidence angle of about 5-15 degrees. Light levels are of the same order of magnitude as earth shine light levels and the moon viewing geometry resembles the nadir observation geometry. The moon is a less favourable calibration target than the sun because moon availability, phase, polarisation, non-uniformities and partial slit filling complicate the calibration. These properties will be discussed in this paper. It will be shown that despite these disadvantages the moon provides a very useful calibration target in addition to the sun. This paper continues the analysis of the GOME moon observations first presented in an earlier paper [Ref 2].

2. ERS-2 orbit and lunar properties

Moon observations are in principle possible on both the day- and eclipse sides of the orbit, but the observations discussed here have all been obtained on the eclipse side. By rotating the nadir scan mirror towards the edge of its total clear field of view (85 deg) the moon can be observed in the field of view of the GOME instrument. The incidence angle on the scan mirror is then about 5-20 deg. The field of view height of GOME is 0.139 deg whilst the moon diameter is 0.52 deg, which shows that GOME measures only about one third of the moon instantaneously. As a result of the satellite orbital movement the field of view (called slit hereafter) moves over the lunar disc. In order to ensure proper moon viewing conditions accounting for satellite pointing instabilities the slit has to move across the moon in such a way that the moon will always be within the field of view in azimuth direction (long slit direction) for the total duration of the observation, while it moves across the slit in elevation direction (short slit direction). In order words, the angle between the moon orbit and the GOME slit long direction has to be large enough to ensure that the moon will not be missed altogether as a result of pointing uncertainties. For GOME this pass angle has to be larger than 22 deg for a useful moon observation. In fact, given the moon viewing geometry, this requirement is so strict that moon observations are only feasible for a small number of specific orbits per year, with the moonphase always being about 0.6, between full moon and last quarter. A more detailed description of GOME moon observations is given in reference 3. A moon observation sequence lasts about 2-4 minutes in total, depending on the exact conditions, i.e. how fast the moon moves over the slit in elevation direction. During this time period several spectra are recorded as the slit moves across the lunar disc, with pixel exposure times of 12 seconds for all 4 detector arrays. Polarisation Measurement Device (PMD) [Ref 1] signals are recorded every 1.5 seconds. The PMD signals thus provide a good way of analysing the moon observation sequence in time. Figure 1 shows the seven different moon observation sequences from 3 september 1996 as monitored with PMD detector #2. It can be seen that depending on moon phase and exact moon orientation with respect to the slit the signal evolution and maximum signal value may vary considerably. In an earlier paper the temporal evolutions of such moon observation sequences were analysed in detail in order to understand and quantify all contributing factors to the moon measured signals [Ref 2]. When single moon spectra are to be compared to the sun-over-diffuser spectra the exact amount of illuminated moon field of view filling during the moon observation needs to be known, since for the sun spectra the diffuser ensures that the complete field of view is illuminated. This geometrical slit filling factor Aslit, which is also important for the moon signal evolution during a moon observation sequence described above, can be calculated if the orientation of the moon arc within the field of view is known from predictions. Aslit is defined as the ratio of the field of view area illuminated by the moon to the total field of view area baz x hel = 2.8 deg x 0.139 deg. As the moon moves across the slit in elevation direction during a moon observation sequence Aslit changes continuously, thus leading to attenuation of the measured signals. The maximum value of Aslit for a particular moon observation sequence depends on the viewing conditions, but typically amounts to 0.13-0.18.

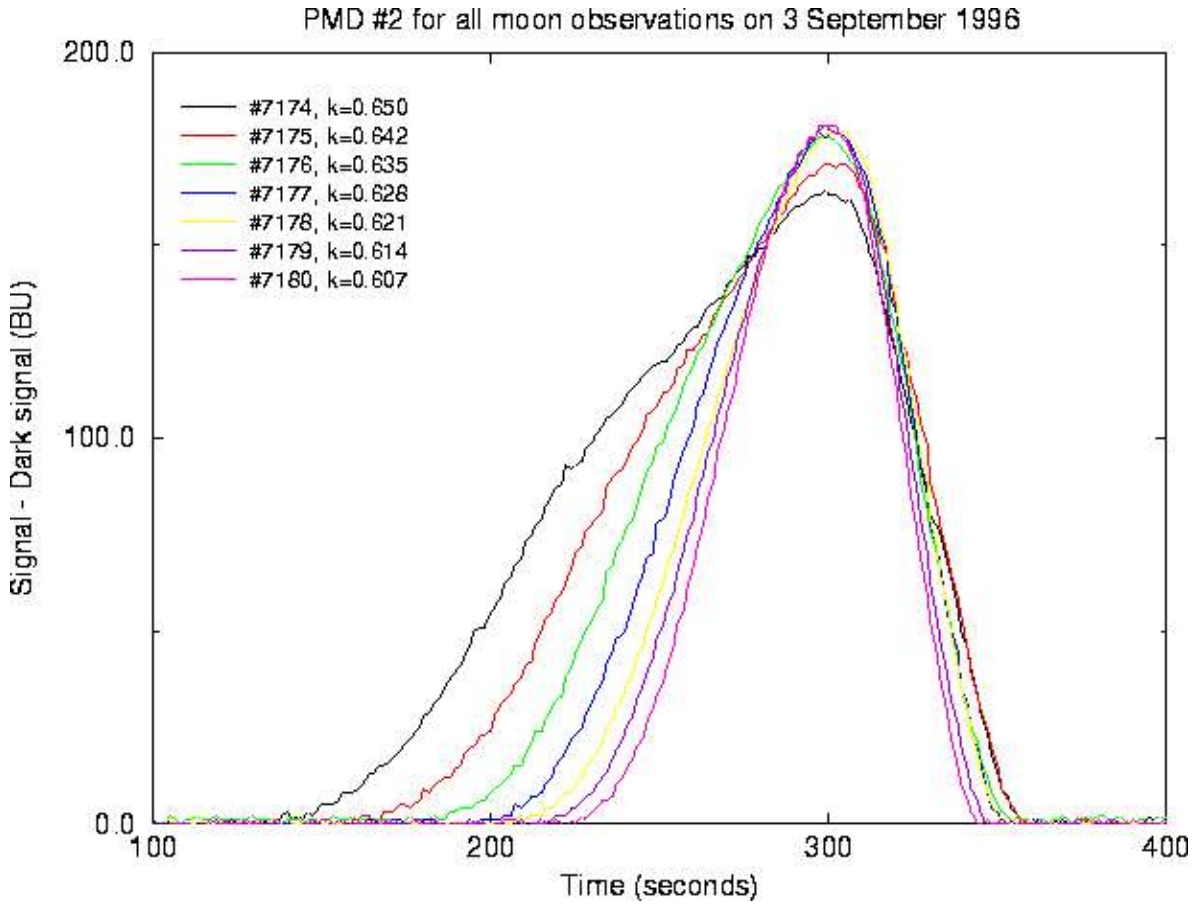

Figure 1: PMD #2 for all moon observations on 3 september 1996.

The signals measured by the detector arrays for the sun-over-diffuser, moon, and earth nadir observations are:

$$S_{sun}(\lambda) = Irr_{sun}(\lambda).T_{mesh}.M_{i=x}(\lambda).Diff(\lambda).M_{i=x}(\lambda).M_{i=x}(\lambda).O(\lambda).PET_{sun}.A_{slit}.h_{si} \qquad (1)$$

$$S_{moon}(\lambda) = Rad_{moon}(\lambda).M_{i=5-20}(\lambda).O(\lambda).PET_{moon}.A_{slit}.D(g).A_{ccd}.h_{si} \qquad (2)$$

$$S_{earth}(\lambda) = Rad_{earth}(\lambda).M_{i=45}(\lambda).O(\lambda).PET_{earth}.A_{ccd}.h_{si} \qquad (3)$$

with S_{sun}, S_{moon}, S_{earth} the measured detector array signals in binary units per second, Irr_{sun} the sun's irradiance in W/cm^2.nm, Rad_{moon} and Rad_{earth} the radiances from the moon and earth in W/cm^2.sr.nm, T_{mesh} the attenuation factor resulting from the solar mesh (0.196), $M_{i=x}$ the coated aluminium mirror reflectivity at incidence angle x (taken polarisation independent), Diff the diffuser efficiency in 1/sr, O the complete remaining efficiency of the instrument, which is the same for the three measurement modes (this includes optics and the detectors) and PET is the detector array pixel exposure time. For the moon observations there is an additional attenuation factor besides A_{slit} discussed above, namely D(g), with g the phase angle of the moon (-180 deg<=g<=180 deg, g="0" deg for full moon, and g="-90,+90" deg for half moon). It is well known that light levels from the moon are very much dependent on the moon phase angle g. This originates from the fact that the illuminated area varies and from the fact that the diffusion incidence angle and exit angles vary. The illuminated area can be described by the moon phase k, which is defined as the ratio of the illuminated lunar disc over the total lunar disc, as seen from GOME or the earth). k and g are related via k="(1+cosg)/2." The total amount of light emanating from the lunar disc integrated moon as a function of the moon phase angle g is shown in figure as I(g). The moon phase k is plotted in the same figure, which has been taken partly from reference Since GOME observed only part of the moon instantaneously and since the moon illuminated area has been accounted for already in Aslit we use the function D(g) to describe the moon diffuser characteristics as a function of the phase angle g, with D(g)="I(g)/k." D(g) is also shown in figure For typical GOME moon observations k="0.6," g="78" degrees and D(g)="0.2.

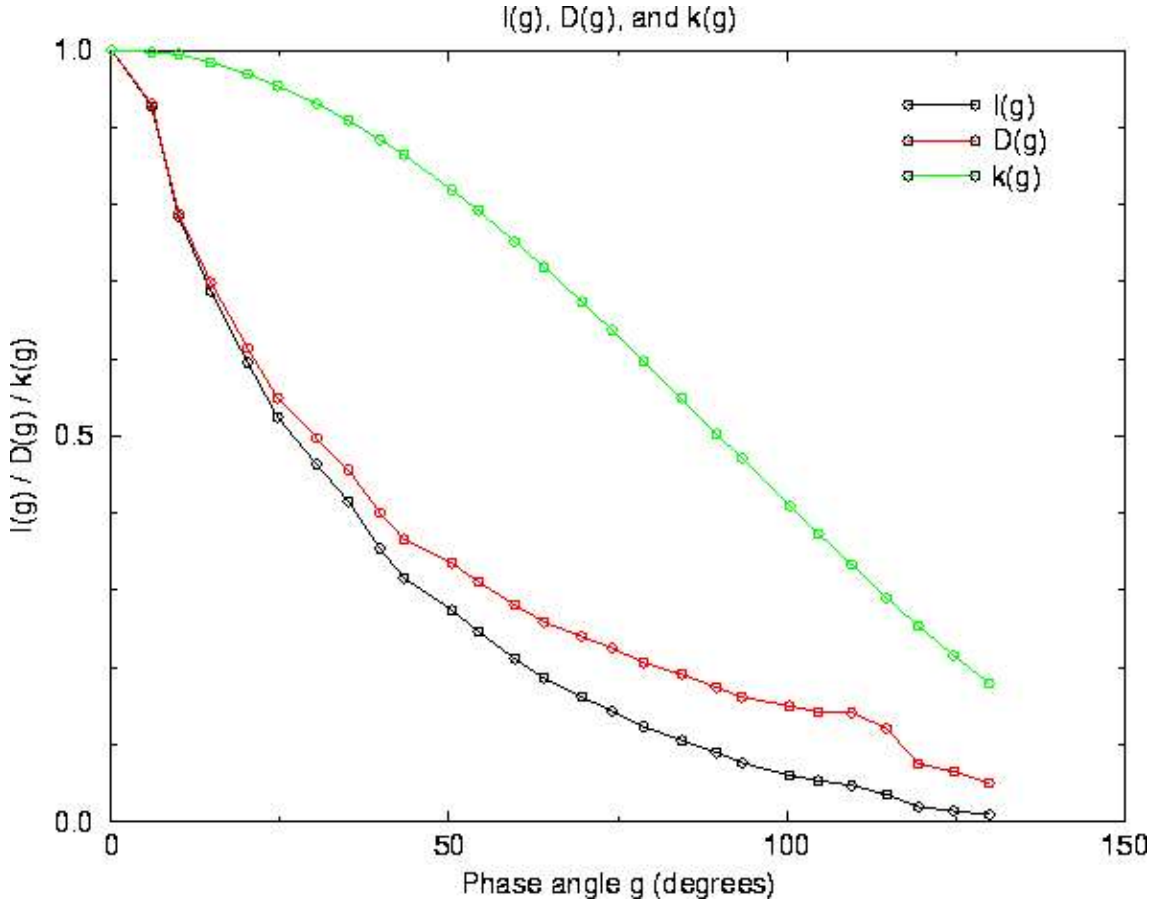

Figure 2: I(g), D(g), and k(g).

(2) describes single moon spectra. For a moon observation sequence Aslit changes continuously and thus (2) must be evaluated for all these cases to describe the complete observation sequence. From signal-to-noise as well as scientific considerations it is desirable to describe the moon signal for the complete lunar disc. This signal is determined by the elevation rate vel, i.e. the speed at which the slit moves over the lunar surface in elevation direction. In fact, the following equation can be derived to describe the complete moon observation sequence:

$$\Sigma(S_{moon}(\lambda))_i = Rad_{moon}(\lambda).M_{i=5-20}(\lambda).O(\lambda).I(g).\pi.R^2_{moon}.(h_{sl}/v_{sl}) \qquad (4)$$

with R_{moon} the moon radius in degrees (=0.26 deg). In (4) A_{slit} and PET_{moon} are no longer present; they are replaced by a new parameter: v_{el} [deg/seconds]. The geometrical albedos for the earth and the moon are defined as:

$$a_{earth}(\lambda) = \pi.Rad_{earth}(\lambda)/Irr_{sun}(\lambda) \qquad (5)$$

$$a_{moon}(\lambda) = \pi.Rad_{moon}(\lambda)/Irr_{sun}(\lambda) \qquad (6)$$

and can be obtained from (1)-(4). Since Rad_{moon} is calculated from (4), (6) describes the geometrical albedo for the complete (illuminated) lunar surface observed during the moon observation sequence. It can be seen that in these albedo ratios of spectra O cancels, which contains the well known and studied etalonning and dichroic shifting features [Refs 4,5]. Ratioing for example moon albedos yields the degradation of the optical components used for the sun observation, but not for the moon observation, i.e. the calibration unit optical components. In order to assess the stability of the instrument ratios of sun spectra obtained at different orbits or days can be examined, if the sun spectra are first normalised to 1 AU to correct for earth-sun distance variation. The moon spectra can also be used for this purpose, provided one can correct for the different values of $M_{i=5\text{-}20}$, v_{el}, and I(g). One obtains:

$$\frac{S_{sun}(\lambda)_1}{S_{sun}(\lambda)_2}.\frac{r_1^2}{r_2^2} = \frac{Irr_{sun}(\lambda)_1}{Irr_{sun}(\lambda)_2}.\frac{(T_{mask}.M_{i=25}(\lambda).Diff(\lambda).M_{i=25}(\lambda).M_{i=22}(\lambda))_1}{(T_{mask}.M_{i=25}(\lambda).Diff(\lambda).M_{i=25}(\lambda).M_{i=22}(\lambda))_2}.\frac{(O(\lambda))_1}{(O(\lambda))_2} \qquad (7)$$

$$\frac{(\Sigma(S_{moon}(\lambda))_i)_1}{(\Sigma(S_{moon}(\lambda))_i)_2}.\frac{r_1^2}{r_2^2}.\frac{v_{sl2}}{v_{sl1}}.\frac{I(g')_2}{I(g')_1} = \frac{Rad_{moon}(\lambda)_1}{Rad_{moon}(\lambda)_2}.\frac{(M_{i=5-20}(\lambda).O(\lambda))_1}{(M_{i=5-20}(\lambda).O(\lambda))_2} \qquad (8)$$

$$\frac{a_{moon}(\lambda)_1}{a_{moon}(\lambda)_2}.\frac{v_{sl2}}{v_{sl1}}.\frac{I(g')_1}{I(g')_2} = \frac{(T_{mask}.M_{i=25}(\lambda).Diff(\lambda).M_{i=25}(\lambda).M_{i=22}(\lambda))_1}{(T_{mask}.M_{i=25}(\lambda).Diff(\lambda).M_{i=25}(\lambda).M_{i=22}(\lambda))_2}.\frac{(\Sigma(S_{moon}(\lambda))_i)_1/S_{sun}(\lambda)_1}{(\Sigma(S_{moon}(\lambda))_i)_2/S_{sun}(\lambda)_2} \qquad (9)$$

with r being the sun-earth distance in AU. In words, (7)-(9) describe the degradation of individual parts of the GOME spectrometer. (7) describes the degradation of the complete spectrometer including the sun-calibration unit, (8) describes the degradation of the

complete spectrometer in the moon mode, i.e. excluding the sun-calibration unit, and (9) describes the degradation of only the sun-calibration unit. By looking at such ratios the instrument component(s) responsible for degradation can be located. (7) and (8) contain O, and thus will show time-varying features such as changing instrument responsivity due to changing etalonning (ice layers on array detectors) and dichroic shifting, which is most apparent in the boundary region between channels 3 and 4 (around 600 nm). The latter effect is caused by instrument outgassing in space, which stabilises slowly with time as the instrument orbital lifetime increases. (9) shows no such time varying features, since O cancels in the moon albedo. The signal-to-noise characteristics decrease quite drastically from (7) to (8) to (9). In the following section the ratios of (7)-(9) will be investigated in order to address the question whether instrument degradation originates from optical components common to both sun and moon observational modes, or from optical components which are part of the sun-calibration unit instead.

3. Results and discussion

3.1 Instrument degradation

In this section we will investigate data from 1995 and 1996 in order to examine possible instrument degradation. Figure 3 shows two sun ratios as calculated from (7) from three dates in July 1995, November 1995, and September 1996. The strong features at 450 nm and 600 nm derive from shifting of the dichroic mirror reflectance characteristics (see above) [Ref 4]. The other oscillations originate from the changing etalon effect [Refs 4,5]. The small-scale rapid oscillations in channel 4 (600-800 nm) have been reported earlier [Refs 2,4] and probably derive from optical interference effects within the solar mesh. It can be clearly seen from figure 3 that towards the ultraviolet the optical efficiency has degraded by about 12% in somewhat over a year. This degradation has also been reported earlier [Ref 4], but the question is which optical component(s) are responsible for the observed degradation. Figure 4 shows similar plots for the moon observations on the same dates, as calculated from (8). For each date three moon observation orbits have been averaged before ratioing and in the ultraviolet some wavelength averaging has been performed to increase signal-to-noise. Again, features from dichroic shifting and etalon change are clearly visible, whereas the rapid small- scale oscillations in channel 4 are absent. The instrument degradation is also clearly visible from the moon spectra: it amounts to about 18% in the ultraviolet in somewhat over a year time. The variation in offset from the two ratios with respect to each other and the difference from unity may derive from systematic errors in vel and I(g). The spectral shape of the ratios is, however, not influenced by these effects. The similarity from the results obtained from sun and moon spectra is further emphasized in figures 5 and 6. Since the moon mode does not employ the sun- calibration unit optics the results from figure 4 seem to suggest that instrument degradation is apparent in the moon mode, which equals the earth-watch mode, i.e. the scan mirror plus the main GOME spectrometer and detectors. Figure 7 shows the ratios of the moon albedos as calculated from (9). First, the moon albedo is calculated for each date (basically moon divided by sun) and then the ratios of different dates can be calculated. For each date four moon albedos from different orbits were averaged and some wavelength averaging was performed in the ultraviolet to increase signal-to-noise. Note that the effects of dichroic shifting and changing etalon are now largely absent in these ratios, although some artefacts persist. Even though the signal-to-noise is not as good as for the previous figures showing sun and moon ratios, the curves from figure 7 seem to suggest that there is efficiency degradation towards the ultraviolet of about 10% in the sun-calibration unit (remember that the moon albedo only contains optics from the sun-calibration unit, see above).

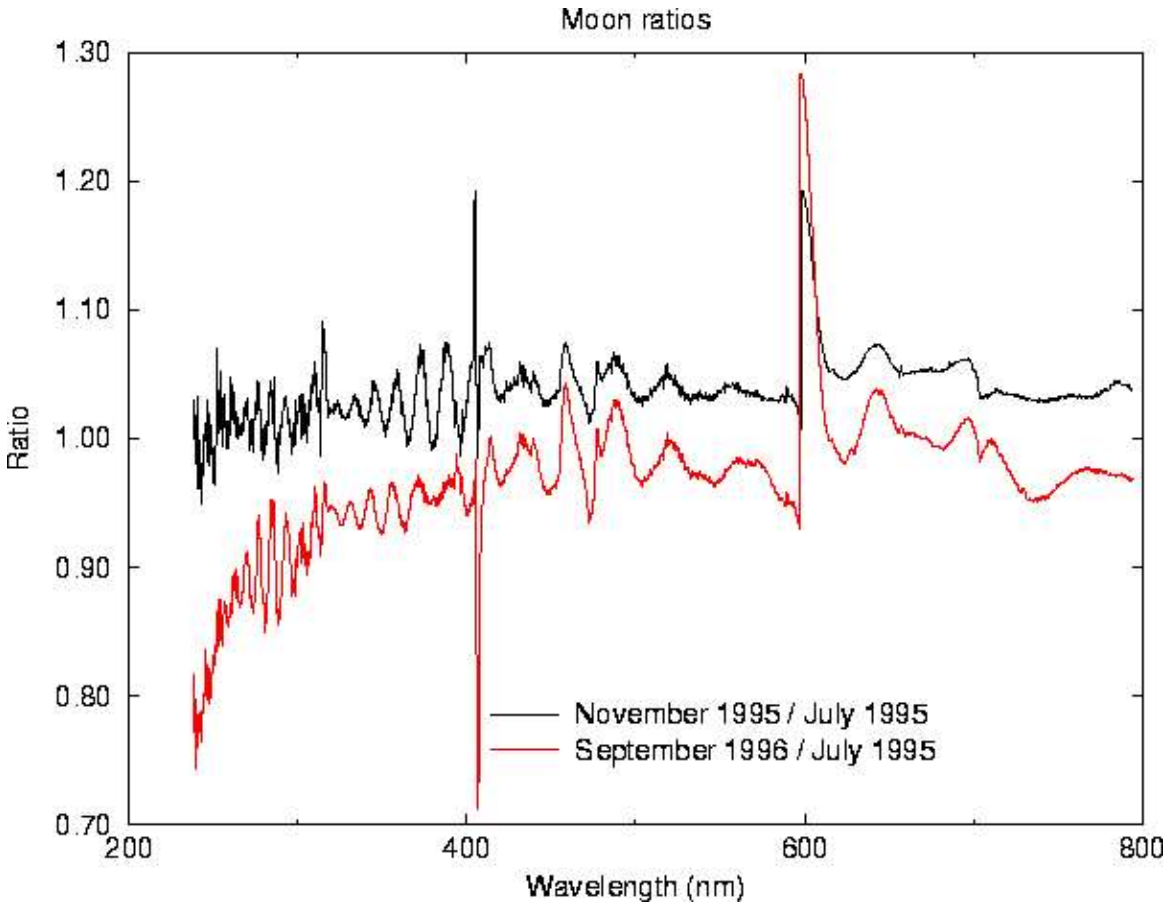

Figure 3: Sun ratios from July 1995, November 1995, and September 1996.

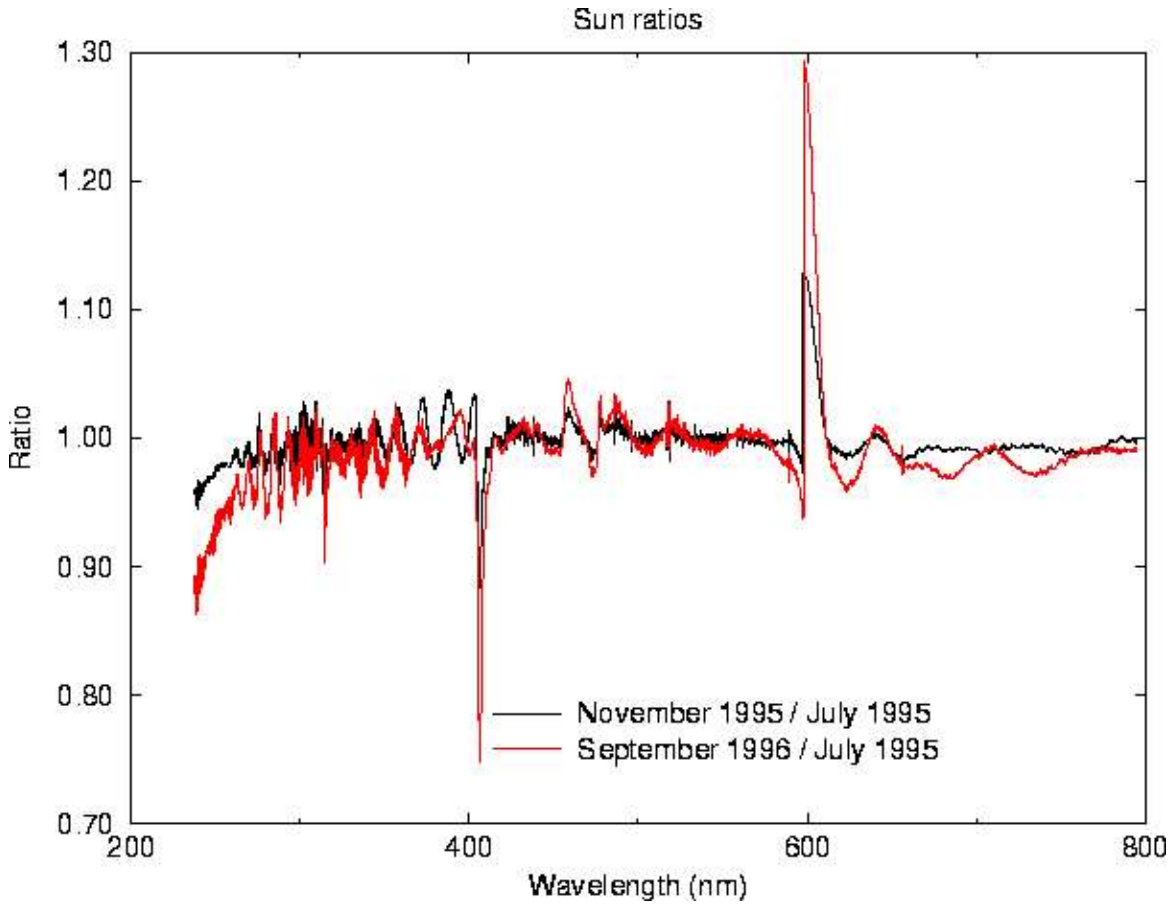

Figure 4: Moon ratios from July 1995, November 1995, and September 1996.

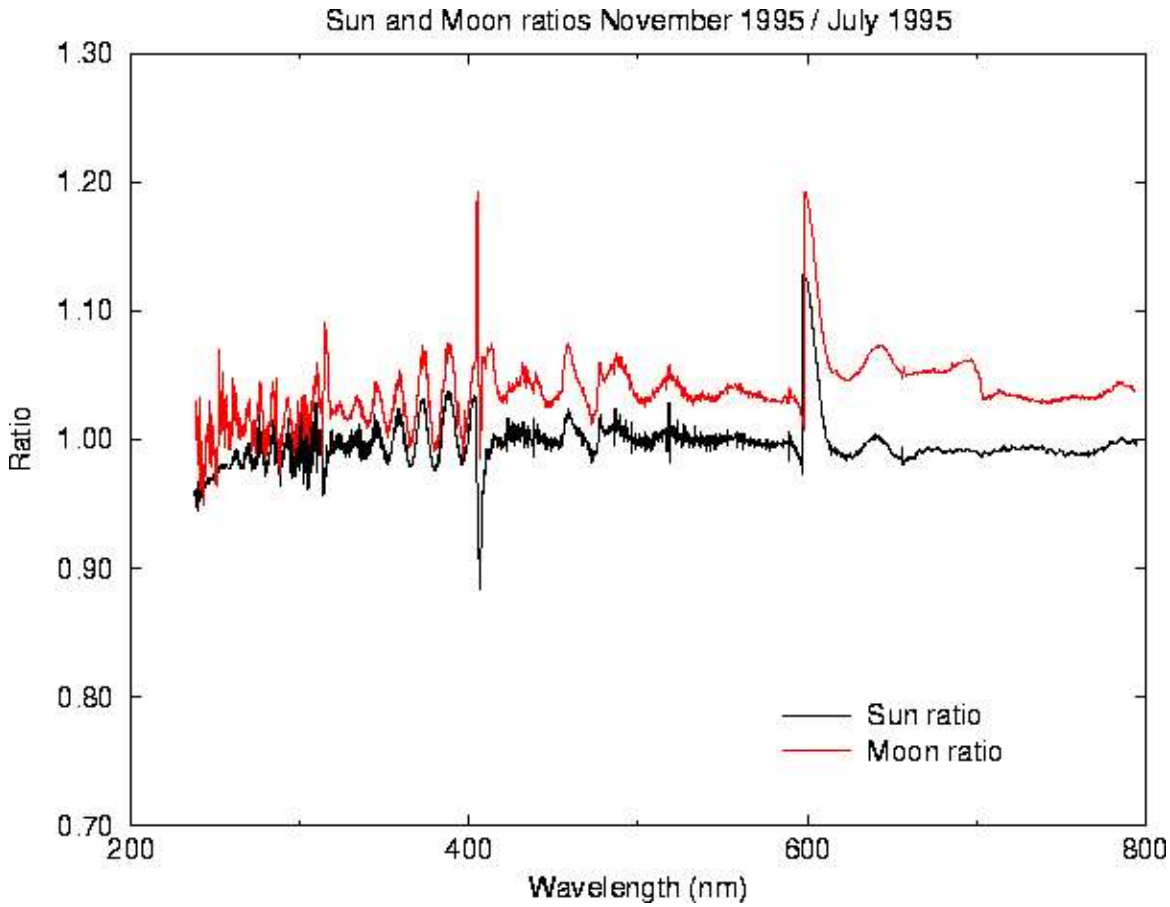

Figure 5: Sun and Moon ratios November 1995 / July 1995.

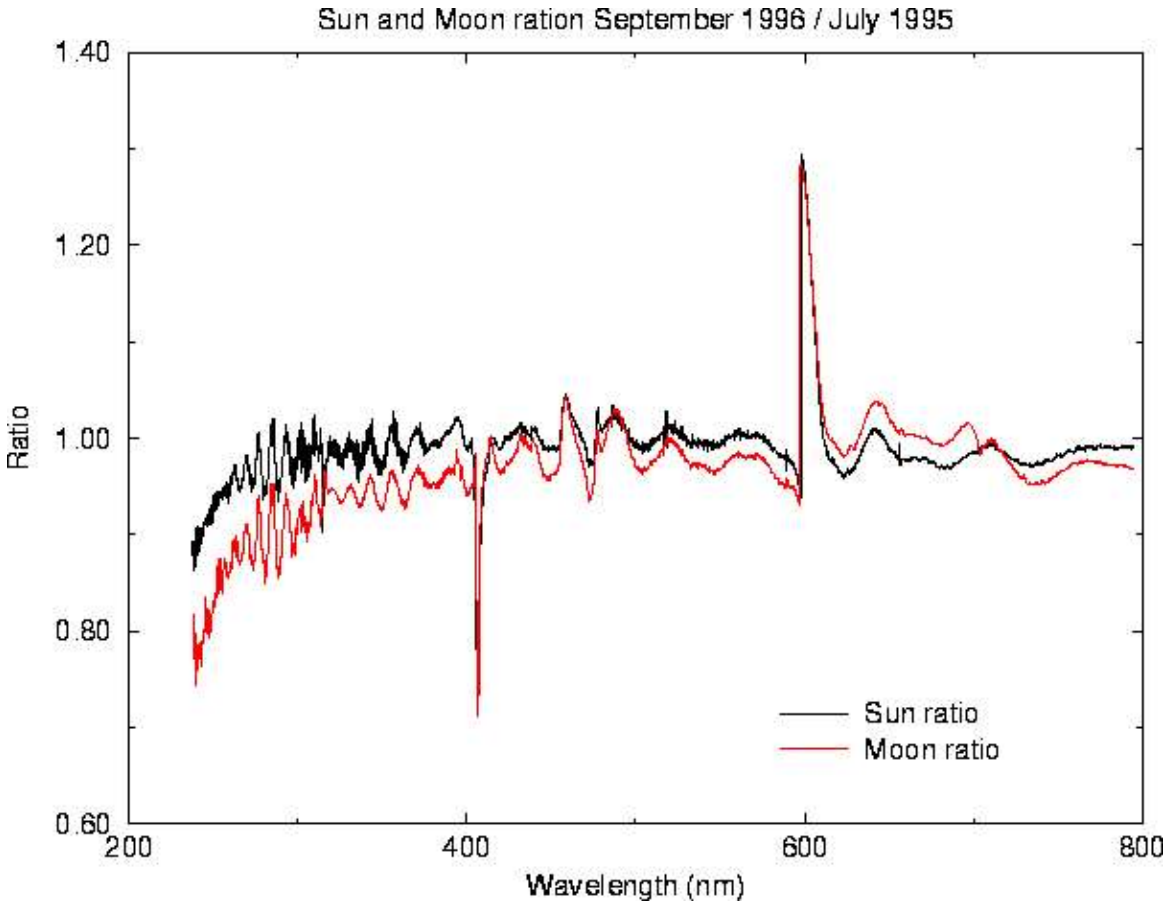

Figure 6: Sun and Moon ratios September 1996 / July 1995.

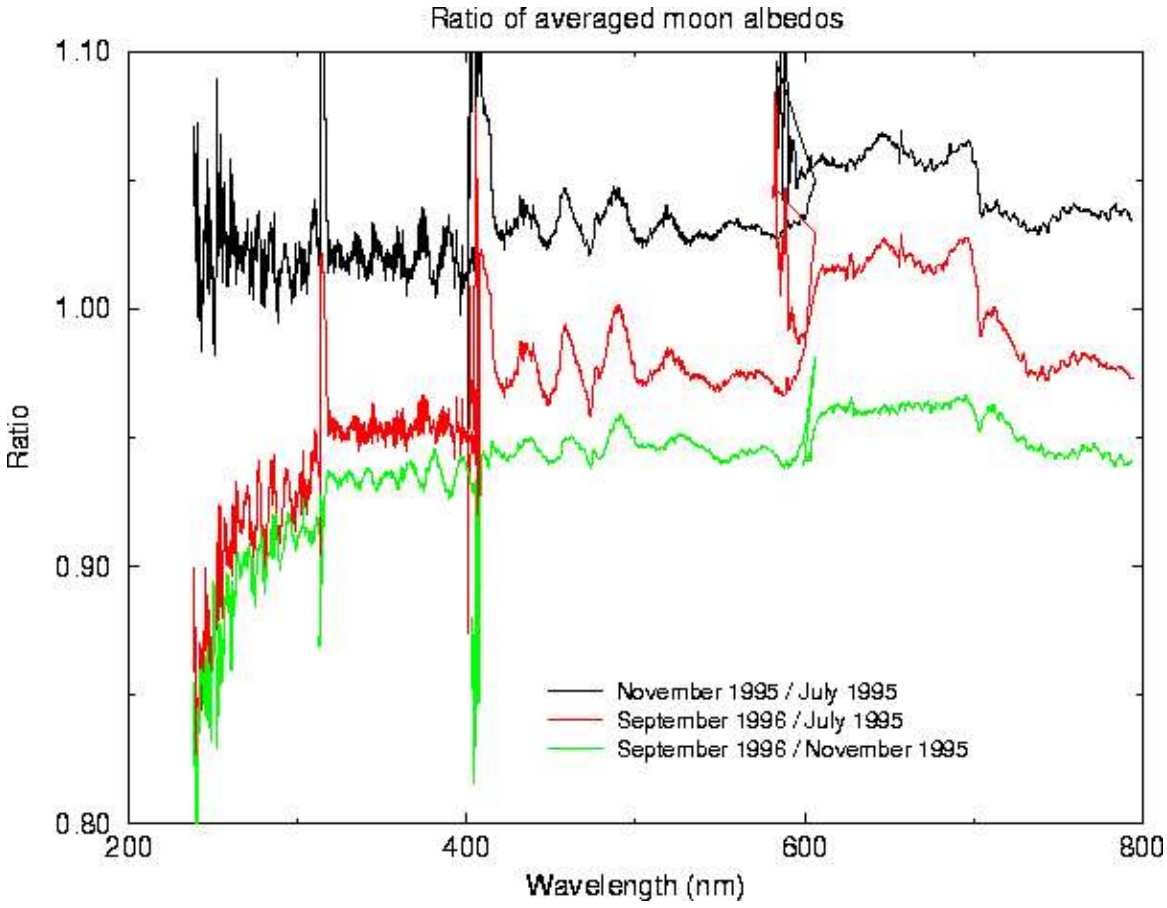

Figure 7: Ratios of averaged geometrical moon albedos.

3.2 Geometrical moon albedo

Figure 8 shows the calculated GOME geometrical moon albedos from a number of dates as calculated from (1), (4), and (6) in comparison with existing literature values obtained from the earth and from SSBUV [Ref 6]. The numbers of orbits indicated in the figure have been averaged to increase signal-to-noise, especially in the ultraviolet. The shown albedos are calculated for the complete illuminated lunar disc at the time of observation. Signal-to-noise values in the ultraviolet of the albedos shown in figure 8 are considerably better than reported previously [Ref 2].

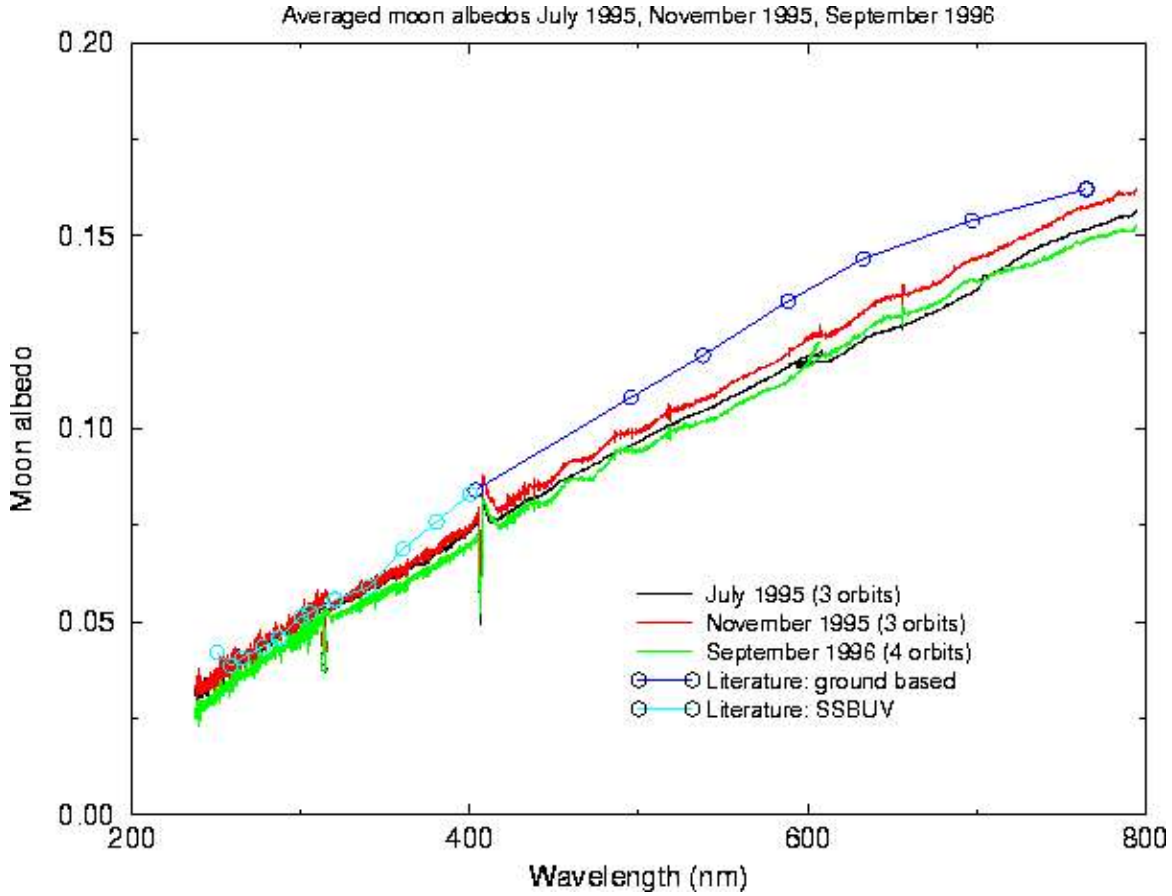

Figure 8: Averaged geometrical moon albedos measured by GOME from July 1995, November 1995, and September 1996.

4. Conclusions

In this paper sun and moon spectra measured by GOME have been investigated in detail, and all relevant factors contributing to these signals have been analysed in detail. It was shown that both the sun and moon spectra can be employed to monitor instrument characteristics like etalonning on the cooled array detectors, changes in the characteristics of the dichroic mirror that separates channels 3 and 4, and overall efficiency degradation over the complete wavelength range. A number of ratios of measured spectra were discussed to investigate efficiency degradation of the various parts of the spectrometer. It was shown that the moon observations provide unique possibilities for instrument monitoring since the moon observations are performed with an instrument configuration that equals the nadir earth observations, whereas the sun-over-diffuser measurements are performed with a different configuration that uses additional components of the sun-calibration unit. The moon spectra seem to imply that it is not merely the sun-calibration unit that is subject to degradation, but the main GOME spectrometer parts as well. The potential of using the moon observations to investigate instrument degradation has been shown, but more measurements are required to obtain better statistics for more definite statements. Finally, the spectrally resolved geometrical moon albedo for the complete illuminated lunar surface was derived for the wavelength range 240-800 nm for the first time.

5. References

[Ref 1] GOME users manual, European Space Agency (ESA), SP-1182, 1995.
[Ref 2] Moon observations with GOME, SPIE proceedings 2831, Ultraviolet Atmospheric and Space Remote Sensing: Methods and Instrumentation,
R.E. Huffman and C.G. Stergis ed., 1996 Denver U.S.A., ISBN 0-8194-2219-3, pages 154-168.
[Ref 3] "Study of the sun and moon as radiation calibration targets", Final report ESA contract number 10346/93/NL/CN, Reference SSF-ESA-SM-0002, July 19, 1994.
[Ref 4] GOME Geophysical Validation Campaign Workshop proceedings, Italy, January 1996, ESA WPP-108 (May 1996).
[Ref 5] G.H. Mount, R.W. Sanders, and J.W. Brault, "Interference effects in reticon photodiode array detectors", Applied Optics 31, pp. 851-858, 1992.
[Ref 6] Observations of the lunar geometric albedo during the ATLAS-3 mission, S.J. Janz, E. Hilsenrath, and R.P. Cebula, private communication.

Keywords: ESA European Space Agency - Agence spatiale europeenne, observation de la terre, earth observation, satellite remote sensing, teledetection, geophysique, altimetrie, radar, chimique atmospherique, geophysics, altimetry, radar, atmospheric chemistry